Chapter 1

INTRODUCTION AND LITERATURE SURVEY

1.1. CLASSIFICATION OF MACHINING PROCESSES

The machining process can be broadly classified as a conventional and non-conventional process. Conventional machining process happens by means of shearing of material through physical interaction of tool and workpiece. This includes processes such as turning, milling, drilling, shaping etc. All these processes will be subjected to high temperature and energy while applied to hard, difficult-to-machine material. This has led to the development of other categories of machining process called non-conventional processes. These are specifically known as advanced machining processes due to its wide scope and application areas. The need for such techniques is due to the development of new and hard materials such as cobalt, chromium, titanium, nickel and its alloys for biomedical and aerospace application which gained lot of interest in the research community [1]. The development of different machining techniques has evolved over the years and its demand is ever increasing from the industry. Some of the commonly used processes are classified based on the material removal mechanism as represented in Figure 1.1. These processes are basically classified according to the type of energy used such as mechanical, thermoelectric, chemical, electrochemical and results in different mechanism of material removal such as erosion, fusion, ablation and ion displacement respectively. The commonalities in all these processes is that the machining of workpiece happens without contacting the tool which eliminates the need of high strength cutting tools and rigid work holding devices. This makes the processes cost-effective and highly suitable for micro and fragile components.

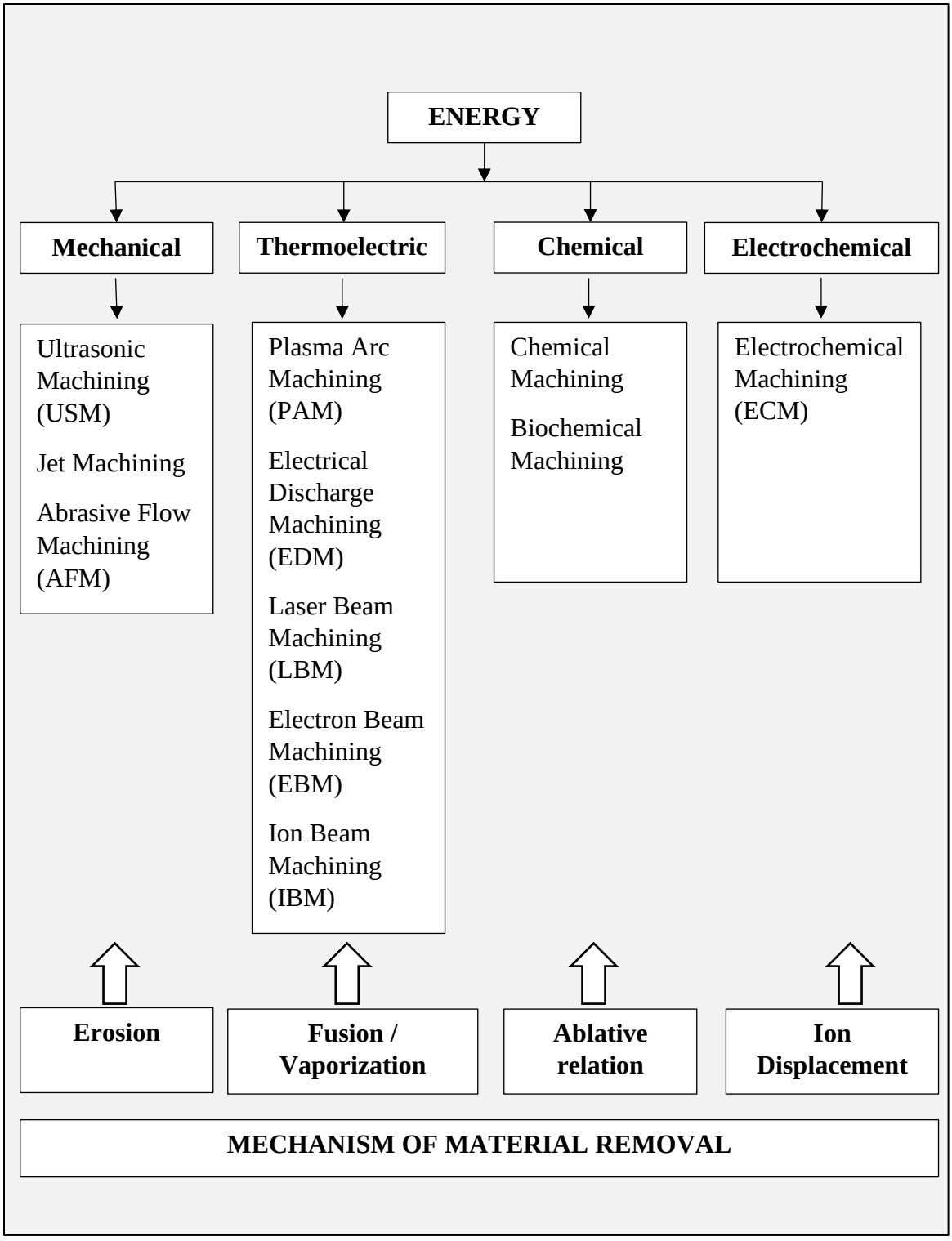

Figure 1.1 Non-conventional machining processes [2]

Today the industries are looking for miniaturization of the components to make the system compact and reduce the energy, materials and improve the system response. The need for microfabrication has grown over the period in the manufacturing sector due to the development of MEMS and microsystems such as micro pumps, micro actuators, micro valves and there has been a continuous search for advancement in machining techniques. The non-conventional processes mentioned earlier can be considered suitable for micro machining because of its unique material removal mechanism which works on non-contact mode and controlled energy transformation between tool and workpiece. However, certain modification in input conditions such as energy, source/diameter, accuracy of motion and precision of system are required to transform the macro-technology to micro-technology. Some examples of micromachining processes are µLBM, µEBM, µEDM and µPAM [3].

A process which has gained lot of importance and being popular among researcher is Electrical Discharge Machining (EDM). This process has been developed in the late 1940s and has a history of nearly 75 years [4]. Different types of EDM processes such as die-sink EDM, wire cut EDM, block EDM and EDM milling has evolved for various applications. EDM has become indispensable in the industry because of its ability to machine complex shapes, achieve high aspect ratio, economical, environmentally friendly and compact system irrespective of the strength of the material. The following paragraph will explain the physical phenomenon of the process for machining hard-to-cut materials.

1.2. ELECTRICAL DISCHARGE MACHINING (EDM)

1.2.1. Breakdown Phenomenon

The EDM process consists of anode and cathode surrounded by dielectric acting as an insulating medium in the gap. The tool acts as a cathode (negatively charged), workpiece acts as an anode (positively charged) and a potential difference is applied across a gap of few microns. When the potential difference reaches a critical value at the narrowest gap, the dielectric undergoes breakdown to cause electrons to break loose from the cathode and move towards anode under the influence of electric field force. This causes the voltage to drop in the gap and increases the flow of current. The breakdown voltage depends on the

electric field, gap length, temperature of cathode and dielectric property. The continuous motion of electrons and protons in the gap creates an avalanche and results in ionization and formation of a plasma channel. The breakdown phenomenon starts with a growth of a thin weakly-ionized channel from one electrode to other called as a streamer as shown in Figure 1.2. The streamer starts to develop from cathode due to an intensive primary electron avalanche as shown in Figure 1.2 (a). The polarization of the charges inside the streamer causes a space charge field to be associated with the avalanche. This electric field increases with the growth and propagation of avalanche. When the space charge field associated with the avalanche exceeds the applied field, a weakly ionized region is created and thus streamer is initiated. The propagation of the streamer towards the anode or cathode depends on the gap distance and applied voltage. When the gap and applied voltage is moderate, the transition from avalanche to streamer occurs towards the anode. However, before reaching the anode the avalanche is not grown enough and the space charge field is not high enough to create an ionized region. Hence the streamer starts from the anode and grows towards the cathode and is called cathode directed or positive streamer as shown in Figure 1.2 (b). The streamer grows due to secondary avalanches created near the positive head of the streamer and these secondary avalanches are initiated by electrons released by photoionization. When the gap and applied voltage is large, the space charge field of the primary avalanche is high and this can create streamer even before reaching the anode that is in the gap. Mostly, the streamer grows towards the anode and is called anode-directed or negative streamer as shown in Figure 1.2 (c). Both the positive and negative streamers grow due to the charges created ahead of its tip by secondary avalanches.

The closing of the gap by streamer completes the breakdown phase and begins with the discharge phase. The intense electric field created near the streamer head and cathode emits a large number of electrons which are accelerated towards anode causing strong ionization. This results in the formation of a plasma channel as shown in Figure 1.3. The plasma channel expands and the surrounding gas is ionized rising the temperature of the spark to about 10000 K and causes high energy density in a small area. The plasma channel is surrounded by the vapor bubble and it grows during the ON cycle of the power supply.

Due to intense heating, the tool and workpiece material is melted and vaporized in the sparking zone. The anode melts first due to the higher mobility of electrons as compared to protons moving towards the cathode. Due to this, the plasma radius at the cathode is much smaller than at the anode.

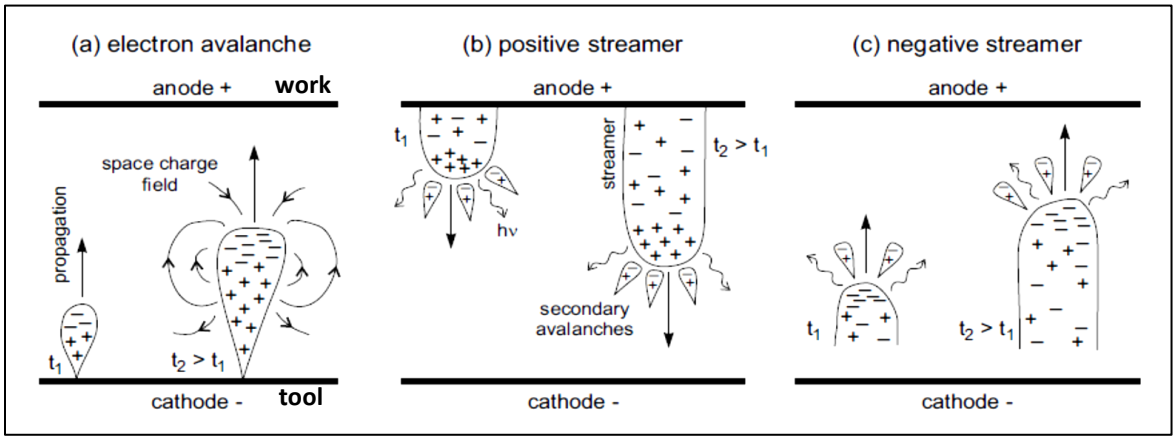

Figure 1.2 Breakdown mechanisms leading to a discharge. Propagation of (a) primary electron avalanche, (b) a positive streamer, and (c) a negative streamer [5]

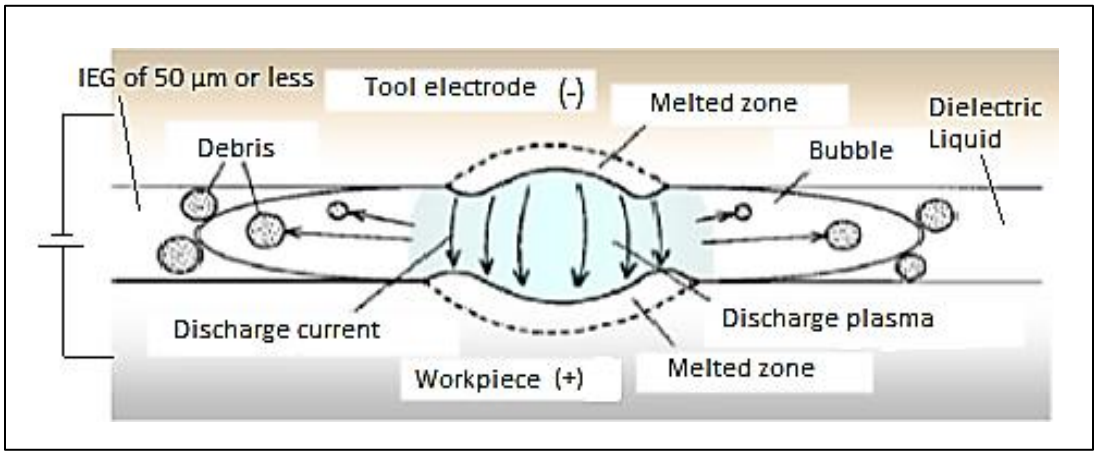

Figure 1.3 Schematic diagram of discharge gap due to multiple discharges [6]

During the OFF cycle, a sudden collapse of the plasma channel and the vapor bubble occurs causing the molten metal from both the tool and the workpiece to expel out. The ejection of metal forms a small cavity on the workpiece and tool which is called a

crater. The size of the crater generated depends upon the input energy and the shape of the plasma channel. The metal carried away by the dielectric cools and get solidify to form debris particles. These debris particles are predominantly spherical in shape due to the surface tension of the dielectric. The process continues with the recovery of the dielectric strength and subsequent sparking in the next cycle. The continuous creation of craters results in the formation of a required profile on the workpiece.

1.2.2. Elements of EDM

The EDM process setup is represented by a schematic diagram as shown in Figure 1.4. The basic elements of the EDM process are power supply, generator, tool electrode, workpiece electrode and dielectric system. The power supply is an important part of the EDM process which generates pulsating supply using either resistance-capacitance (RC) circuit or transistor circuit. The ZNC generator provides automation to EDM system and controls the servo mechanism to maintain a constant gap. The oscilloscope is used to display and analyze the waveform of the electrical signals which can be stored and retrieved using data recorder.

The tool is shaped as the negative replica of the required profile to generate the final shape machined on the workpiece. The commonly used tool electrode materials are copper, brass, graphite and tungsten. Any hard electrically conductive material can be used as a workpiece. The important properties needed for the electrode materials are high conductivity, high thermal diffusivity, high melting and boiling point. The dielectric plays an important role in the EDM process. The dielectric acts as an insulating medium and is responsible to generate a spark between the two electrodes. It also serves various functions such as cooling of electrodes, controlling the shape of plasma channel and removal of debris particles. The tool and workpiece are submerged in the dielectric tank and the fresh dielectric is supplied continuously. The dielectric at a high velocity is circulated near the sparking zone through nozzle for enhancing material removal.

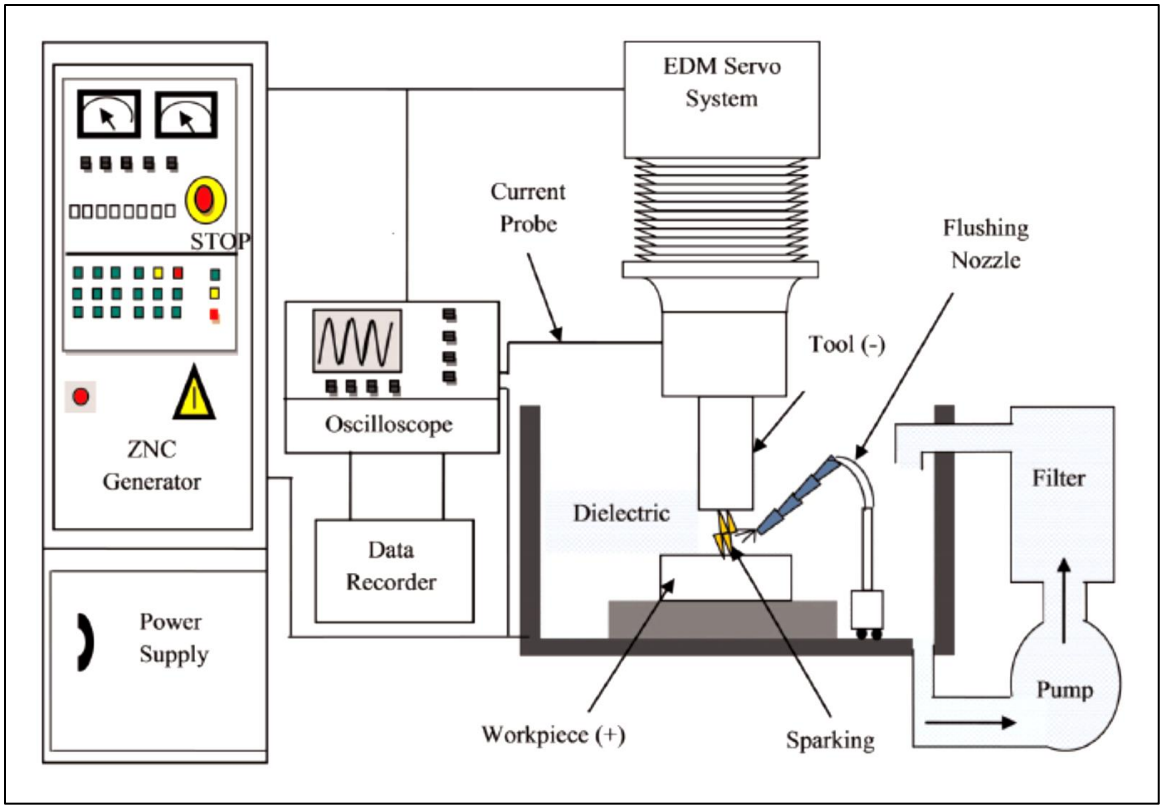

Figure 1.4 Schematic diagram showing EDM setup [1]

1.2.3. Properties of different dielectric

The dielectric is broadly classified into three categories namely oil based, water based and gaseous. The various types of dielectric used in EDM are mineral oil, kerosene, mineral seals, transformer oil, distilled water, distilled water with additives, and gaseous dielectric [7]. The selection of dielectric is based on its physical properties such as dielectric strength, dielectric constant, electric conductivity, viscosity, specific heat, thermal conductivity, density and boiling point. The physical properties of different dielectric fluids are listed in Table 1.1. The following paragraph will elaborate the importance of each dielectric property. First important property is the dielectric strength which refers to the ability of the fluid to maintain high resistivity before spark discharge and to recover rapidly after the discharge. It is the measure of the insulating capacity of the dielectric fluid. It is known that, after the dielectric breakdown, discharge plasma decays

and results in emission of shock waves which is subsequently followed by decay of the vapor bubble.

Table 1.1 Physical properties of kerosene, deionized water, and air

Physical Property	Kerosene	Deionized water	Air
Dielectric strength (MV/cm)	1	0.7	0.03
Dielectric constant	1.8	80	1.02
Electric conductivity (μs/cm)	0.015	1.33	5×10^{-11}
Kinematic viscosity (cm^2/s)	1.16×10^{-2}	0.852×10^{-2}	0.148
Specific heat (J/kg^0C)	2100	4200	1.005
Thermal conductivity (W/mk)	0.14	0.62	0.016
Density (kg/m^3)	860	100	1.29
Boiling point (^0C)	200	100	-

The electric recovery of the dielectric depends on time required for removal of bubbles since dielectric strength of gases or vapors is lower than that of liquids. High dielectric strength reduces the discharge gap and increases the current density improving the material removal rate (MRR). Observing the Table 1.1, it is apparent that the dielectric strength of kerosene is more as compared to water and air which makes a suitable candidate for many EDM processes. The second property similar to dielectric strength is dielectric constant or permittivity (ε). The dielectric constant is the ratio of ability of material to carry the current to the ability of vacuum to carry the current. It is a dimensionless constant that indicates how easy a material can be polarized by the imposition of an electric field on an insulating material. The third property of the dielectric is the electric conductivity. The higher width of the discharge channel provides more energy and removes more amount of material. The electric conductivity of the water is more and due to this the discharge channel expands. This enhances MRR but creates a rough surface. The fourth property is viscosity; dielectric with low viscosity has better flowability which improves the flushing characteristics and provides better dimensional accuracy. The dielectric of 2 to 3.5 centistoke (cSt) is suitable for finishing operations and of range 4 to 6.5 cSt is suitable for

roughing operations. The fifth property under discussion is the flash point. The flash point is the lowest temperature at which a dielectric will ignite in the presence of small flame or spark. It is safe to have a dielectric with a higher flash point but it may affect the surface roughness due to proportional increase in viscosity. Properties such as thermal conductivity and specific heat enhance the heat carrying capacity of the dielectric from the discharge area and lead to lower thermal damage.

1.2.4. Impurities in dielectric

The dielectric must be free from moisture and contaminants. The choice of a liquid dielectric mainly depends on its chemical stability. The liquids are easily contaminated and hence has low breakdown strength. The main impurities in liquid dielectric are dust, moisture, dissolved gases and ionic impurities. The presence of dust particles reduces the breakdown strength of the liquid dielectric as it gets charged due to electric field. If a single conducting particle is present in the electrode gap it increases the local field. When this field exceeds the breakdown strength of the liquid, the local breakdown occurs near the particle and this results in the formation of gas bubbles eventually causing breakdown of the liquid. Increase in the size of the particles, lowers the breakdown strength. The particles present in the dielectric experiences the force due to difference in permittivity of two materials and the applied field. When large number of such particles are present, they get aligned due to these forces and form a stable chain bridging the gap and causing a dielectric breakdown. The dielectric oil is more susceptible to impurity such as fine droplets of water suspended in it. The presence of small amount of water reduces the dielectric strength of the oil considerably. The dissolved gases such as oxygen, carbon dioxide also affects the dielectric strength of the liquids. The ionic impurity such as water vapor gets easily dissociated which leads to very high conductivity and heating of the liquid depending on the electric field.

1.2.5. Comparison of commonly used dielectric

In die-sink applications, hydrocarbon oils are more efficient than distilled or deionized water [8]. Kerosene has better insulation properties and hence used in precision

machining. Kerosene is a chemical compound consisting of hydrogen and carbon which decomposes at high temperature during sparking and forms carbide layer on the work surface and also forms carbon (tar) particles. Similarly, deionized water produces an oxide layer on the work surface. As the melting point of carbide is larger than oxides, large discharge energy is needed to remove material using kerosene as compared to deionized water. Likewise, the impulsive force of discharge in kerosene is unstable which cause reduction in the MRR. The hard carbide layer also forms over the tool surface and forms a protective layer against tool wear. Due to this, the tool wear using kerosene is less than that while using the deionized water. The major problem with kerosene is a low flash point and high volatility which may lead to fire hazards [9]. The average diameter of debris particles machined in deionized water is larger than that machined in kerosene. The deionized water has better processing performance than kerosene and urea solution. It improves MRR, lowers tool wear rate (TWR), improves surface finish but with poor accuracy [10-12]. The deionized water is environment-friendly, but the use of deionized water can damage the machine parts due to corrosion. The recast diameter of crater increases with increasing pulse duration irrespective of the type of dielectric used. This is due to the conduction of heat in the material and expansion of the discharge plasma. The recast diameter and depth of crater is bigger while using oxygen than in air due to the oxidation reaction between the molten metal and oxygen. The material removal process is also affected by the pressure of discharge generated bubble. At low external pressure, craters with a flat molten surface without central depression are formed, whereas, at high external pressure, several central depressions surrounded by rim are formed due to the flow of molten metal out of the crater. This causes higher material removal efficiencies in liquid dielectric than in gaseous dielectric. The expansion and contraction of the discharge generated bubble exert an impulsive force on the tool and workpiece. This impulsive force is larger in liquid dielectric than in gaseous dielectric due to higher density and viscosity of the liquid dielectric [14]. The machining characteristics of various dielectric fluids are listed in Table 1.2.

Table 1.2 Machining characteristics of different dielectric fluid [7-8] [13-14]

Hydrocarbon oil	Deionized water	Gaseous dielectric
• Efficient in die sink applications. • Surface roughness is higher. • The microhardness of the white layer is higher due to the higher content of carbon. • Hydrocarbon oil used are mineral oils, kerosene, mineral seal and transformer oil. • Prone to fire hazards and it decomposes to form carbon black, benzene (C_6H_6), benzopyrene ($C_{20}H_{12}$), acetylene, ethylene, hydrogen, carbon dioxide, carbon monoxide.	• Higher performance and environmentally suitable than hydrocarbon oil. • Surface roughness is lower. • Thicker workpiece heat affected zone with a higher concentration of microcracks. • Higher MRR but poor machining accuracy. • Lower tool electrode wear ratio. • Tap water, deionized water and water-in-oil emulsion is used. • Substances generated are water vapor, carbon monoxide, nitrogen oxide, ozone, and chloride.	• Higher MRR than hydrocarbon oil. • Tool electrode wear ratio is very low. • Gases used are oxygen, nitrogen, air, helium and argon. • Substances generated are fluorite, chlorite, nitrite, bromide, nitrate, phosphate, sulphate, carbon dioxide, ozone and carbon monoxide.

1.3. MICRO ELECTRIC DISCHARGE MILLING (µED-MILLING)

The µED-milling process uses a simple cylindrical tool rotating at high speed to produce the desired shape by following a programmed path. The schematic diagram showing the comparison between die-sink EDM and µED-milling with respect to tool motion is shown in Figure 1.5. The micro tool is fitted vertically in the spindle and is fed towards the stationary workpiece clamped on the machine vice. The servo control system maintains the constant gap and the continuous spark generated in the gap melts and vaporizes the material along a predefined path. The spark is generated along the periphery and the bottom of the tool. The name ‘µED-milling' has emerged due to the generation of complex shapes by simple cylindrical tool cutting along the trajectory of the tool as in the conventional milling process. The process has advantages similar to EDM such as

machinability of hard materials, high aspect ratio, surface finish etc. However, the tool wear and large machining time are the major concern as in EDM process. In spite of this, the µED-milling process is economical, environmentally friendly and is widely used in micromachining domain for fabricating micro-devices.

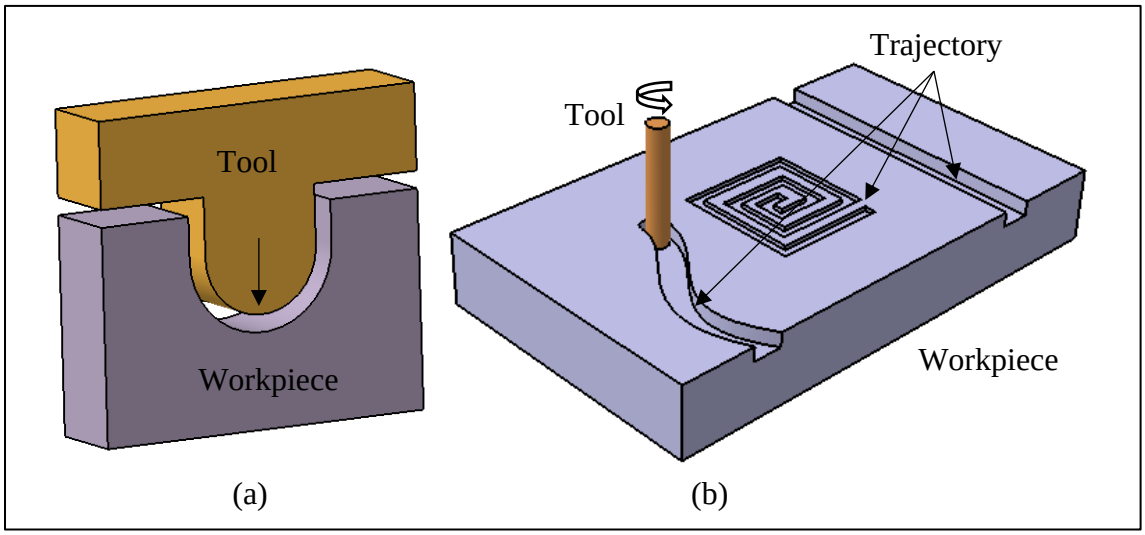

Figure 1.5 Schematic diagram showing tool motion in (a) die-sink EDM and (b) µED-milling

1.4. LITERATURE SURVEY

The EDM process has evolved over the years and a lot of research and development has been carried out in the last two decades. This has resulted in a huge resource of literature on the EDM process and its variants. The present study is focused on the phenomenon occurring at the IEG of µED-milling process and the various topics relevant to it. The CFD simulation and experimental high-speed images of the µED-milling process is captured. The literature survey is presented in five parts which will cover EDM/µED-milling, debris particles, high-speed imaging, simulation of flow-field in the gap, and improvised tool.

1.4.1. EDM/µED milling

The µED-milling process is the variant of the EDM process and it was introduced in 1980. Over the last 25 years, the research has been primarily focused on improving the machining efficiency and exploring the application areas where it can be used with ease as compared to other EDM process.

Modica et al. [15] compared µED-milling and sinking in the fabrication of microchannels (µchannels) on a hardened steel workpiece. The µEDM sinking is 10 to 20 times faster than milling, but it is less accurate than milling due to tool wear which is not compensated during the process. In addition, the manufacturing time to produce the tool in µEDM sinking is one-third to that required to manufacture tool diameter in µED-milling. Nguyen et al. [16] presented the issues in using the present conventional milling CAM software for µED-milling of 3D shapes. By considering the tool wear and the machining gap, the present CAM software can be used for µED-milling. The process involves different steps such as CAD modeling, machining parameters selection, tool path generation, slicing, tool wear calculation, and post-processing.

Han et al. [17] proposed a novel high-speed EDM milling using moving electric arcs. The pipe-like tool electrode rotates at high speed generating moving electric arcs between the gap and removing the material in the form of milling. The material is removed continuously without discharge intervals improving the machining efficiency. Kou et al. [18] proposed a sustainable manufacturing method of high-speed EDM milling. The moving electric arc provide large energy as compared to conventional EDM due to lower rate of short-circuit. The MRR increases by about five times to that of conventional EDM. The increase in the tool speed to 3000 rpm reduces the tool wear. The thickness of re-solidified layer can be controlled by increasing the energy of moving electric arcs.

Wang et al. [19] developed in-situ pulse monitoring system in µED-milling to better understand the process dynamics. They proposed a combined off-line and in-line adaptive tool wear compensation method to achieve effective tool wear compensation in precision µED-milling. Bissacco et al. [20] investigated tool wear and material removal per discharge by discharge counting and volume measurement of material removed from anode and

cathode in μED-milling. With the decrease in discharge duration, the ratio between cathode and anode wear is decreasing irrespective of the discharge energy. Maradia et al. [21] investigated the presence of carbonaceous layer built-up on the tool electrode during the erosion process of EDM. The micro-sized debris particles embedded in this carbon layer increases the hardness of the layer and it has low thermal conductivity which results in lower tool electrode wear.

Uhlmann et al. [22] investigated the use of novel tool material such as boron doped CVD-diamond (B-CVD) and polycrystalline diamond (PCD) in micro die-sinking EDM. The relative wear is less while using B-CVD and PCD as compared to copper, tungsten copper and graphite. Hence, further investigations are needed to check the feasibility of these materials.

Schubert et al. [23] demonstrated the μED-milling of non-conducting zirconia (ZrO_2) ceramics. The machining is carried out by applying a thin layer of silver varnish (45% silver) on the zirconia. During operation, this layer is machined and a conducting rebuilt layer is generated on the workpiece which is responsible for further machining.

Bai et al. [24] analyzed three phase flow dielectric mediums consisting of gas, liquid and powder on the machining performance of the EDM. The output parameters are MRR, TWR and surface roughness (SR) and the input variables include peak current, pulse on time, pulse off time, flow rate and concentration of powder. The three levels of each input variables as low, medium and high is required to improve the machining performance of the EDM. Wang et al. [25] proposed a high current density ED milling for machining Inconel 718. A novel high current density power supply consists of pulse generator with high voltage and a DC power source with high current. The plasma channel is maintained by the DC power source irrespective of the switching off the pulse generator. When the peak current is 920 A, the maximum MRR is 15062 mm^3/min with the relative electrode wear ratio (REWR) of 1.73%. The increase in the dielectric pressure increases the MRR and reduces the REWR.

1.4.2. Debris particle

The byproducts of the EDM basically consists of the micro and nano-sized debris particles. These debris particles create a lot of problems in the μED-milling process. The effective flushing of debris from the gap is essential for smooth machining and hence various authors have used different techniques to study the trajectory and properties of the micro sized debris particles. Rajurkar et al. [26] presented a theoretical study of debris formation and ejection mechanism. The size of a debris particle is derived using the drop formation energy and the kinetic energy of the ejected debris particle. The velocity of the ejected particle is obtained on the basis of analysis of hydrodynamic propagation of shock waves generated due to dielectric breakdown. The radius of the debris particle depends on the surface tension of the molten metal, fraction of the total energy in the plasma, specific gravity of workpiece and the velocity of ejected particles.

Kunieda et al. [27] calculated the debris particle motion in the gap caused by the electrostatic force in EDM using dielectric fluid. The debris particle moves from one electrode to other repeatedly due to electrophoresis. The current carried by a particle is 8.53×10^{-11} A and this can be used to estimate the number of particles in the gap by measuring the leakage current during the discharge delay time. In another study, [28] it is found that numerous chains of debris particles grow in the gap and this is the main reason for the occurrence of the discharge as compared to the gap width. The first discharge does not affect the location of the second discharge as long as the plasma formed from the first discharge has deionized. The minimum discharge interval necessary for the deionization of the plasma is 6 μs. Schumacher et al. [29] proposed that contamination of gap due to eroded debris particles influences ignition, discharge location, and gap width. The discharge is difficult to start in very clean liquid and the bridges of particles enhances discharge. The subsequent discharges can be fired more quickly if larger exposure surfaces are present.

Wang et al. [30] analyzed the mechanism of debris and bubble exclusion during consecutive pulse discharges. Figure 1.6 shows the debris and bubbles excluded from the discharge zone. The effect of electrode jump height and speed on the debris and bubble

movements in the gap is studied. It is observed that the debris exclusion from the gap is mainly due to the bubble expansion movement. In addition, the electrode jump height and jump speed above a certain value are necessary for decreasing the debris concentration from the bottom gap. In another study, authors [31] have proposed that the increase in the discharge current and pulse-on time increases the ability of the bubbles to exclude the debris from the gap. Zhao et al. [32] proposed that the linear motor equipped die-sink EDM is more stable. In a deep and narrow hole or slot machining, the fast electrode motion can remove all debris particles from the gap, eliminating the occurrence of harmful irregular sparks in the gap. Murray et al. [33] proposed that debris reattachment on the tool does not occur randomly but is dependent on its remelting in the dielectric by the secondary discharge process. The flushing of debris from the gap is important to prevent contamination of the dielectric and increasing the possibility of sparking in the same location repeatedly, which can cause damage to the workpiece. The debris can become electrostatically polarized, resulting in secondary discharge by creating favorable discharge conditions on the sides and non-working areas of the electrodes as shown in Figure 1.7.

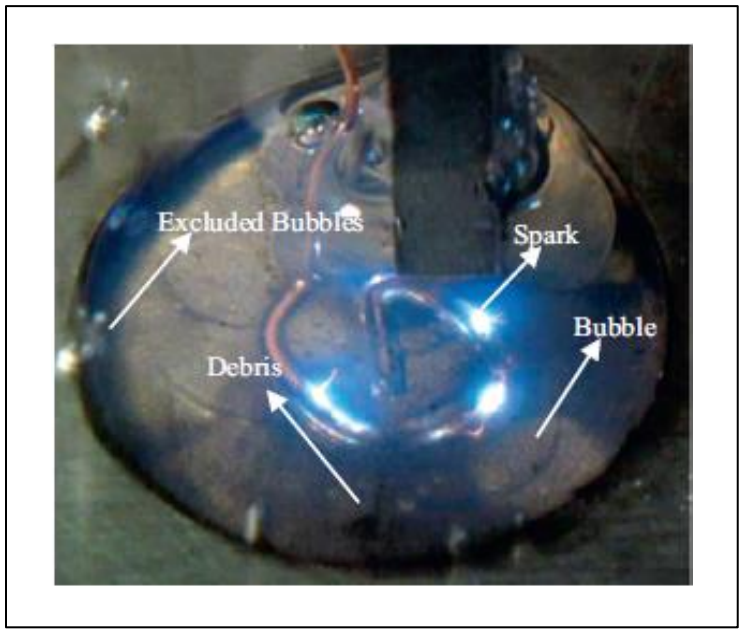

Figure 1.6 Discharge status at electrode down time of 0.24 s [30]

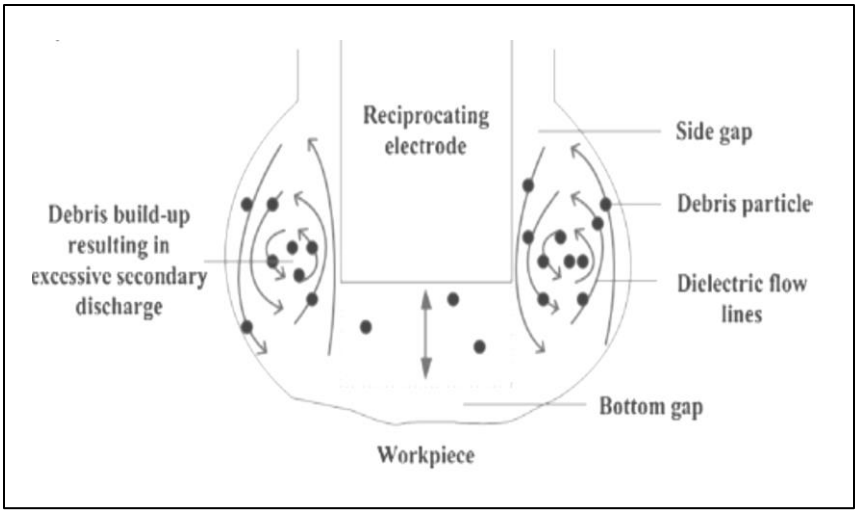

Figure 1.7 Schematic of debris movement in the side gap resulting in secondary discharge [33]

Wang et al. [34] proposed the combined flushing with high pressure dielectric inside the tube electrode and the high velocity dielectric outside the tube electrode for fast hole EDM drilling. In case of blind hole, the pressure of dielectric inside the tube electrode is responsible for debris flushing from the gap. While in through hole, the external flushing has more effect on flushing the debris. The debris concentration is reduced by 94 % and processing efficiency improved by 89 % with the use of external flushing as compared to without external flushing. The combined flushing improved the quality of edges of hole with less machining time.

Tanjilul et al. [35] presented a simultaneous flushing and vacuum-assisted debris removal system which improves debris flushing for deep-hole EDM drilling. A hollow electrode and the suction pump are used to improve the flushing. Surface roughness improved due to suction-assisted drilling. The size of the debris particles depends on the machining current and the debris size increases with the increase in the machining current. Chuvaree et al. [36] proposed an innovative method of flushing technique in deep hole EDM drilling. The flushing through electrode and multi-hole interior flushing was preferred than side flushing. The machining time reduced by 26 % while machining 50 mm depth hole. In addition, the rotation of the tool improved MRR by 35 %.

1.4.3. High-Speed Imaging

The high-speed camera is an effective tool to study the phenomenon at the micro level. It is widely used to study the flow behavior in microfluidics. Researchers have used high-speed video camera images with high frame rates to study the phenomenon happening at the IEG of EDM process. Okada et al. [37] investigated the dielectric fluid flow and debris motion in wire EDMed kerf using simulation and compared with the high-speed video camera images. The images are captured at 500 frames per second (fps) and the observation area was 5×5 mm. The stagnation area was observed around the wire and the authors found that the jet flushing from the upper and lower nozzles was inefficient in the removal of debris from the machined kerf.

Kitamura et al. [38] observed the expansion of plasma in the EDM gap using a high-speed video camera MEMRECAM HX-3, nac Image Technology Inc. The SiC and Ga_2O_3 single crystals were used as the electrode material as they are optically transparent and electrically conductive. The authors observed that the heat source diameter is smaller than the plasma diameter but larger than the crater diameter. Macedo et al. [39] recorded and measured plasma expansion in dry EDM by a high-speed imaging technique. The behavior of the plasma expansion in air and argon is shown in Figure 1.8. Light emission spectroscopy is used to analyze plasma and was done using an Acton Research Spectrograph 0.275 m connected to a high-speed camera Vision Research Phantom V12.1 having a frame rate of 1,00,000 fps and the exposure time of 300 ns. Larger plasma expansions are observed when gas discharges are triggered by streamers as compared to the sparks generated from vacuum breakdown mechanism.

Ayestaa et al. [40] captured different debris evacuation method in slot EDMing for straight and inclined slots. The debris motion was recorded using a high-speed camera Olympus i-Speed LT and it was observed that debris evacuation is difficult in straight slots as compared to inclined slots due to gravity force acting on the particles. The debris accumulated in the slot corners is shown in Figure 1.9. The continuous flushing with a high electrode jump is necessary to improve debris flushing from the gap. Liao et al. [41] investigated the electrode jump motion with different jump heights and speeds to study the

fluid flow and debris fluid interaction in die-sink EDM using the high-speed video camera images of the process. The high-speed camera SV9M001C EPIX with the maximum capture rate of 500 fps is used to capture the flow of debris during the electrode jump motion. They found that the debris flushing is effective when the electrode jump height is larger than one-fourth of machining depth and the jump speed is near the critical speed of bubble generation.

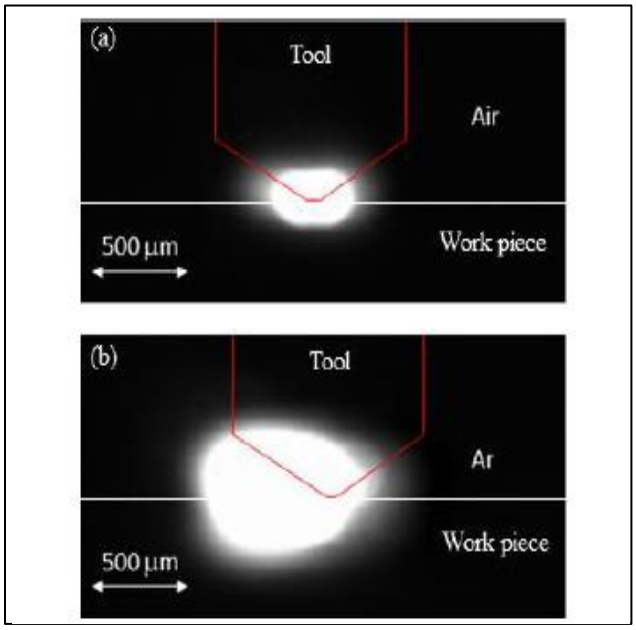

Figure 1.8 Plasma expansion in (a) air and (b) argon [39]

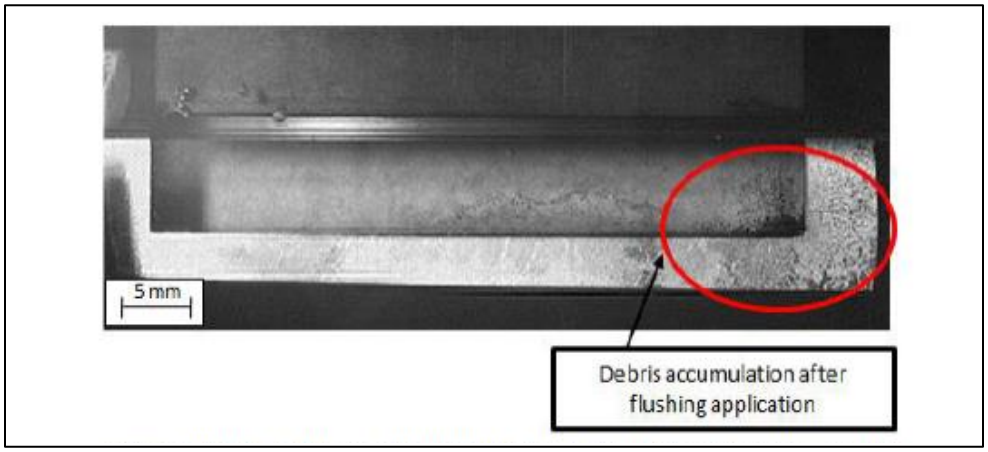

Figure 1.9 Debris accumulation in slot corners after continuous flushing [40]

Hayakawa et al. [42] observed the moment of material removal from a discharge spot using a high-speed video camera. The images are captured with a maximum frame rate of 1,00,000 fps and the exposure time of 10 μs. The observation of the images revealed that the debris particles are removed intermittently during or just after the discharge duration. During the discharge, small debris particles are removed at high flying speed while after the discharge large debris particles are removed at low flying speed.

Takayuki et al. [43] observed material removal process in a single discharge using high-speed camera with a high magnification lens. The Keyence high-speed camera with 2.3×10^5 fps and exposure time of 1.11 μs was used. The high magnification lens of 100× and working distance of 85 mm was used. In a single discharge, material removal occurred several times with the pulse duration exceeding tens of microseconds. The cycle of material removal process consists of heating of material, scattering of material due to evaporation, new surface creation and reheating.

Kliuev et al. [44] used high-speed imaging technique to study the dielectric fluid flow trajectory in EDM drilling. The Phantom v12.1 high-speed camera with high magnification lenses of 1000× is used to capture the images. An internal confocal light with an external source is used to visualize the bubbles and particles. The movement of dielectric mainly depends upon the machining conditions prevailing while drilling a planar surface or a large aspect ratio hole. In deep hole machining, the debris remains in the erosion area and does not get flushed easily.

1.4.4. Simulation

The simulation is a useful tool to study the physical phenomenon of the process and is used by various researcher to study the flow-field, variation of different parameters in the domain under study. The availability of specialized software with well-defined algorithms makes it easy to model and simulate many engineering problems and compare with experimental results. Yeo et al. [45] analyzed and compared five thermoelectric EDM models from Snoeys, Van Dijck, Beck, Jilani and DiBitonto in terms of temperature distribution, crater geometry and material removal at the cathode. DiBitonto used point

heat source model and all others used disk heat source model. Hence, the isotherm surfaces for DiBitonto's model is semi-circular while for other models it is bowl shape with a large ratio of crater diameter to depth. DiBitonto's model showed better agreement with experimental data as compared to other models. Kalajahi et al. [46] used Finite Element Modeling (FEM) to predict the thermal behavior and material removal mechanism in EDM process. Several factors such as temperature dependent material properties, shape, and size of the heated zone, energy distribution factor, plasma flushing efficiency and phase change are considered in thermal modeling. The Gaussian heat flux is used to model the heat in the gap and the energy distribution factor for the cathode is calculated as 5 %. The proposed model shows close agreement with the DiBitonto's model and experimental results to predict MRR with respect to discharge power up to 1100 W.

Mujumdar et al. [47] presented a melt-pool model to predict the material removed from the workpiece (anode) in a single discharge of μEDM process. The fluid flow and heat transfer equations are solved to model the melt-pool and a level-set method is used to find solid and liquid fractions of the workpiece material. A 2D axisymmetric domain is solved using COMSOL multiphysics software. The simulation results showed that the diameter of the discharge crater was 78-96 μm and crater depth was 8-9 μm for discharge duration of 2 μs. Tang et al. [48] established the thermo-hydraulic coupling numerical model of single discharge crater formation and analyzed with FEM. This model couples the heat conduction and fluid flow equations to solve the electrode material removal process. The level set method in COMSOL multiphysics software is used to track the solid/liquid interface formed at the crater surface. The material removal efficiency was 0.04 with most of the molten metal getting re-solidified.

Yang et al. [49] analyzed the material removal mechanism in EDM using molecular dynamics. They proposed that the material removal mechanism in EDM happens in two ways; one by vaporization and the other by the bubble explosion of superheated metals. When the power density is low, vaporization plays the primary role and the material is removed mostly in the form of single atoms; whereas when the power density is high,

bubble explosion plays the dominant role and the material is removed mostly in the form of clusters.

The computational fluid dynamics (CFD) analysis is also used by different researchers to study the dynamics of the dielectric flow in the gap in terms of pressure, velocity, temperature field in the gap which is responsible to improve the flushing efficiency of the process. Haas et al. [50] used dielectric fluid flow simulation in the gap of the wire EDM process to study the flushing efficiency. The study is used to design and analyze dielectric injection nozzles of the wire EDM process for improving the cleaning process in the gap. The k-ω shear stress transport (SST) with low Reynold's number correction and semi-implicit method for pressure-linked equations (SIMPLE) algorithm is used in ANSYS Fluent to perform the simulation. The vortex is observed between the nozzle and the upper surface of the workpiece. When the spark frequency and power are high the machining speed is mainly governed by hydrodynamics. In another study, Pontelandolfo et al. [51] investigated the dielectric fluid flow and particles motion in the gap of die sinking EDM process. A CFD analysis was used to know the size, shape, and kinematic properties of the electrode. Three different 2D geometries and a 3D geometry is used to analyze the flow and the Lagrangian frame-work is used to track the particles in the gap. The velocity of the electrode jump and the jump height are important to remove the particles from the gap. The vortex generated at the bottom of the gap enhances the evacuation of particles. In addition, the lower viscosity of dielectric fluid increases the flushing efficiency.

Mohammad et al. [52] investigated the effect of ultrasonic vibration of the tool, velocity fields, and pressure distribution in the dielectric fluid around the bubble in EDM using the numerical simulation. The pressure inside the bubble is obtained by the unsteady Bernoulli's equation in Lagrangian form and the velocity around the vapor bubble in the liquid domain is obtained by the Green's integral formula. The ultrasonic vibration of the tool has a great effect on the evolution of the bubble, fluid behavior and the efficiency of the machining in EDM. The fluid just near the liquid jet of the bubble have the highest relative velocity. Das et al. [53] introduced for the first-time vapor bubble dynamics and

periodic heating to consider heat absorption by vapor bubbles in EDM. The thermo-electric simulation model of EDM is used to calculate the heat carried by the vapor bubbles from the eroded zone after every spark. About 50 % of the spark energy is absorbed by tool and workpiece due to conduction, 33 % energy is carried away by flushing, 2 % of energy is consumed during vapor accumulation and remaining 16 % is used in metal erosion.

Fujiki et al. [54] investigated the effects of electrode lead and tilt angles and dielectric fluid flow rate on machining performance in near-dry ED milling process. The CFD simulation is used to predict the optimum values of the input variables which affects the machining. The air-kerosene mixture is simulated using volume of fluid (VOF) with implicit scheme. The speed and volume fraction of the fluid is shown in Figure 1.10. The results showed that MRR is linearly proportional to mist (liquid + air) flow rate and TWR and efficiency is inversely related to the mist flow rate. Likewise, increase in the electrode tilt angle reduces the MRR and increases the TWR. Zhou et al. [55] investigated a new method for machining lens molds using tilt ED milling. As compared with the conventional flat-end electrode, the spherical electrode was used. As the dielectric fluid plays an important role in ED milling, its flow change due to spherical electrode is analyzed using simulation. The flat end electrode restrained the dielectric while the spherical electrode provides better flushing effect. The surface roughness reduced by 60 %, MRR improved and the surface quality of the lens mold was optimum at 25^0 tilt angle.

Lunardelli et al. [56] used CFD simulation to design the nozzle used for atomized spray cooling system in micromachining application. The droplet flow simulation is used to study the effect of initial droplet velocity, gas velocity and the angle between two inlets. The Eulerian-Lagrangian multiphase method with a one-way coupling is used to analyze droplet delivery at the cutting zone. The eccentric design of nozzle overperformed the concentric nozzles in terms of cooling and lubrication.

Masuzawa et al. [57] proposed a new method of dynamic jet flushing with moving nozzles that sweep along the outline of the EDM gap. The control volume method which is a type of finite difference method and a SIMPLE algorithm is used for calculation. The sweeping

jet flushing was effective for even distribution of debris in the gap and consequently obtaining the flat surface.

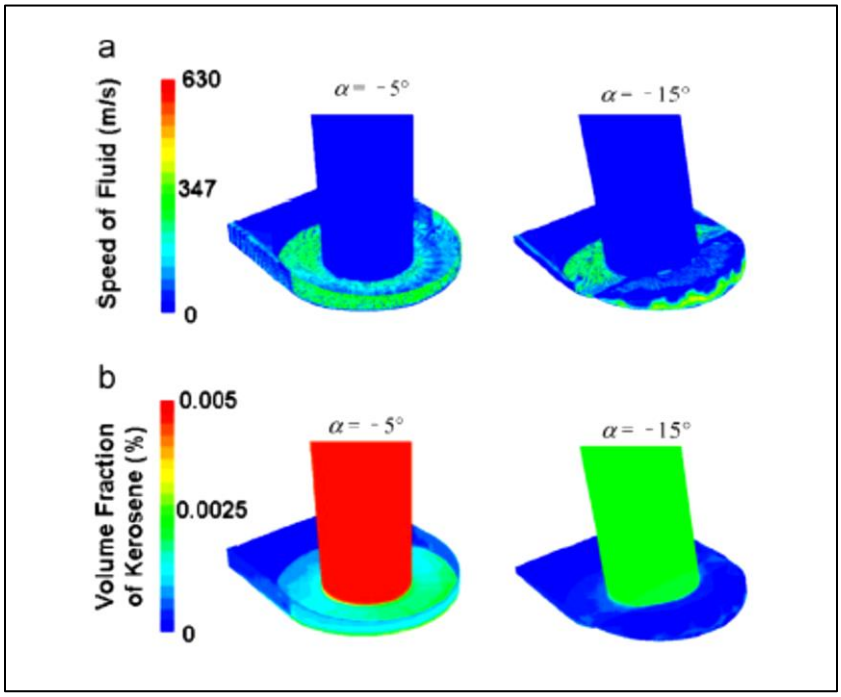

Figure 1.10 CFD simulation results for (a) fluid speed, and (b) volume fraction of kerosene for lead angle of 5^0 and 15^0 [54]

Okada et al. [58] investigated the effect of nozzle jet flushing on wire breakage in wire EDM. The simulation was performed with STAR-CCM+ software. The dielectric flow, debris movement and pressure distribution in the gap is calculated using finite volume method as an unsteady turbulent flow with k–ε model. The Lagrangian liquid–solid flow model is used to track the debris particles. With the increase in jet flushing the deflection of wire increases, accumulating the debris at the particular short kerf length which increases the frequency of wire breakage.

Dilip et al. [59] numerically simulated the crater surface profile formed on Inconel 718 showing the effects of material movement in the mushy zone using μEDM. Figure 1.11 shows the crater geometry and the simulated temperature profile and volume fraction of the mushy zone. Melting and solidification module is used for simulating the molten metal

during discharge. The Gaussian heat flux, Maragoni stress and fixed percentage of heat to anode is applied. The solidus and liquidus temperature are defined to simulate the melting process. The prediction of the crater radius by simulation deviated the actual by 5 % and the crater depth by 10-17 %. The surface profile prediction was 8-13 % comparative to experimental results.

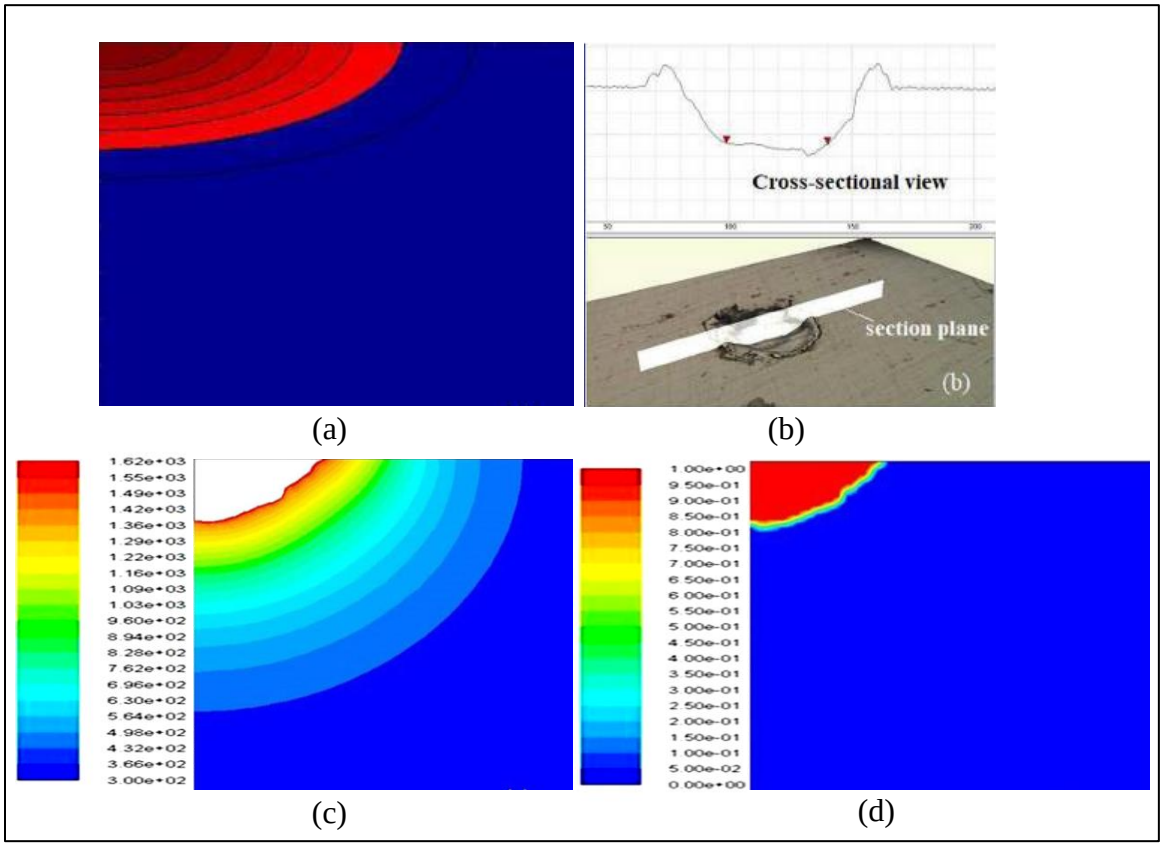

Figure 1.11 (a) Numerically simulated crater geometry, (b) actual crater geometry, (c) temperature profile and (d) liquid fraction at 150 V, 0.4 μF [59]

Gadeschi et al. [60] computed the heat transfer between the workpiece and the dielectric fluid during a flushing cycle of EDM using numerical simulation and experimentation. A thermographic camera and thermocouple are used to obtain temperature measurements which are used as a boundary condition in numerical simulation. The two-phase solid-liquid flow is simulated using a cut-cell liquid-set method for particle simulations. The

debris particles affect the turbulent kinetic energy enhancing fluid mixing which results in the increase of heat transfer rate.

Beigmoradi et al. [61] studied different types of tool geometry and materials which can be used as a vibratory tool electrode in micro-EDM process. The FEM is used to find the mode shapes and the frequency response of circular, quadrangular and triangular tool shape for dynamic force of 1 N and the frequency range from 0 to 6 kHz. The CFD simulation using finite volume method and the standard k-ε model is used to study the dielectric flow in the gap. The velocity was maximum during upward motion of the tool and was better for debris flushing. The vortex generation and the tool shape can enhance the debris flushing in the gap. The tungsten triangular electrode provided best flushing due to lower lateral movements caused due to excitations.

Oezkaya et al. [62] investigated the effect of coolant pressure and diameter of coolant channels inside the tool while drilling Inconel 718. The coolant flow caused due to complex drilling process is simulated using fluid structure interaction (FSI) and CFD. A k-ω SST turbulence model was used in Ansys CFX software. The effect of increasing the coolant pressure was significant as compared to increasing the channel diameter. The pressure induced higher flow rates enhanced the heat transfer rate, increased tool life due to better internal cooling.

Kliuev et al. [63] investigated the effect of drilling conditions on pressure and dielectric flow during EDM drilling using simulation. Electrodes with internal flushing channels are used to increase debris flushing. The effect of electrode diameter, gap, configuration of the flushing channel, electrode length and drill depth are analyzed. The standard k-ε turbulence model is used for finding the flow-field. Figure 1.12 shows the dielectric flow velocity and turbulent kinetic energy at the outlet of the multi-hole electrode. The debris flushing efficiency is improved by internal flushing channel diameter and its configuration. This enhances the MRR and reduces the recast layer thickness.

Mihic et al. [64] used CFD simulation to study the fluid flow in the grinding process. The distribution of temperature, pressure, velocity, liquid volume fraction and the flow patterns in the domain was analyzed. Figure 1.13 shows the velocity vector in the grinding region.

The standard k-ε turbulence model with standard wall functions and the Eulerian mixture multiphase model is used in Ansys Fluent to model the two-phase air-water mixture. The determination of the flow patterns in the machining zone was useful to study the wasted flows and the grinding process. The flow-field obtained using simulation would be difficult to obtain using experimental method.

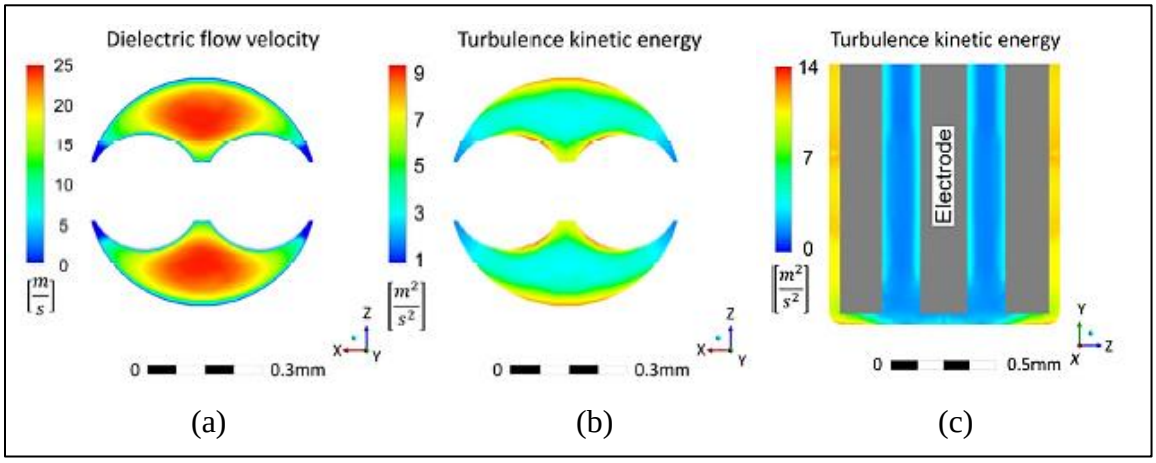

Figure 1.12 (a) Axial flow velocity distribution at the outlet, (b) turbulence kinetic energy at the outlet and (c) turbulence kinetic energy plot in cross-section of YZ plane [63]

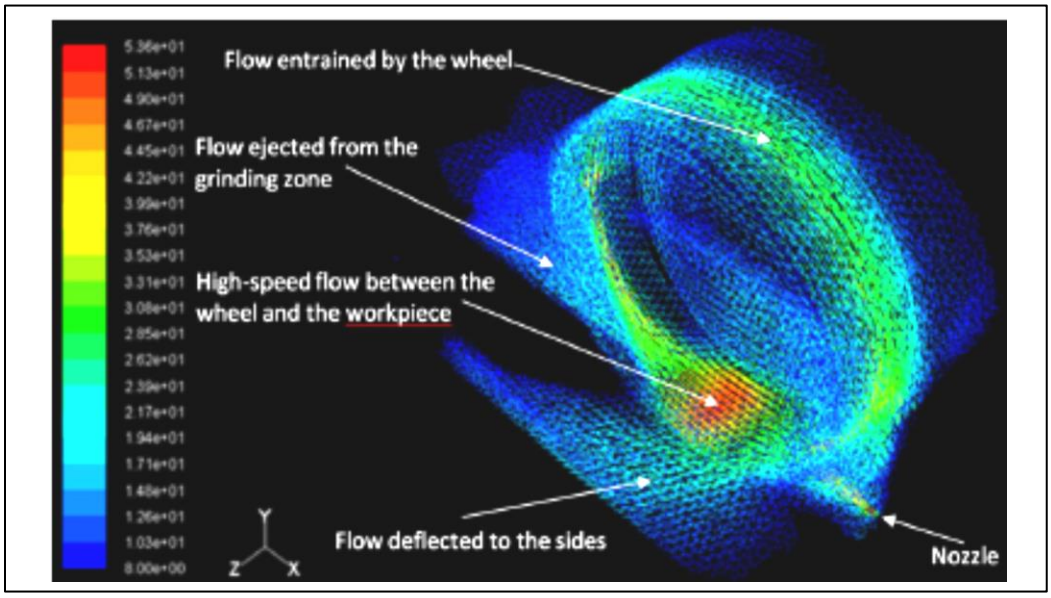

Figure 1.13 Velocity vectors of liquid colored by velocity magnitude (m/s). Range of velocity vectors shown: 8 m/s to 53.6 m/s [64]

Yu et al. [65] studied the effect of ultrasonic vibration on suspension flow-field in ultrasonic polishing. The CFD is used to simulate the velocity, pressure and the behavior of polishing suspension in the base fluid which is Newtonian fluid. The VOF model is used to simulate the solid-liquid two-phase flow. The dynamic mesh model and SIMPLEC algorithm is used for simulation. The flow-field of pressure and velocity below the polishing head followed the sine and cosine rule respectively. The ultrasonic polishing improved the polishing efficiency and reduced the surface roughness to 4 nm as against 15 nm without ultrasonic vibration.

1.4.5. Improvised tool

Various techniques have been developed by different researchers to improve flushing efficiencies such as high electrode jump and improvised tool. In this aspect, a simple cylindrical tool is modified to improve flushing and machining performance. Various types of tool geometry used by researcher is shown in Figure 1.14 and its performance in machining is presented here. Flano et al. [66-67] found an alternative method for SiC slicing using foil electrode. The foil electrode is selected as its thickness can be made smaller than the wire diameter. However, large side surface area of the tool causes secondary discharge on side surface increasing debris concentration and affecting the kerf width accuracy. Hence, two foil electrode designs; a foil with side holes and a foil with side insulation is proposed and tested. The machining stability improved due to effective flushing of debris and reduction of side surface discharges. The authors also studied the geometry and position of the holes machined on the lateral faces of the electrode. The observed holes or flushing pockets on the electrode penetrate the entire machining depth.

Nastasi et al. [68] utilized slotted tools for Electrical Discharge Drilling (EDD) of high aspect ratio holes to improve MRR. The MRR enhanced by 300 % using slotted tools as compared to cylindrical tools. Slotted tools enhanced debris flushing from the gap. Ferraris et al. [69] developed an innovative method for the EDD of high-aspect-ratio micro holes using insulated tubular tool electrode. The micro-holes of 0.2 mm diameter and aspect ratio

of 120 is obtained by preventing secondary sparks due to coated tools. The aspect ratio increased by 30 % and the tool wear decreased by two times as compared to the normal tools.

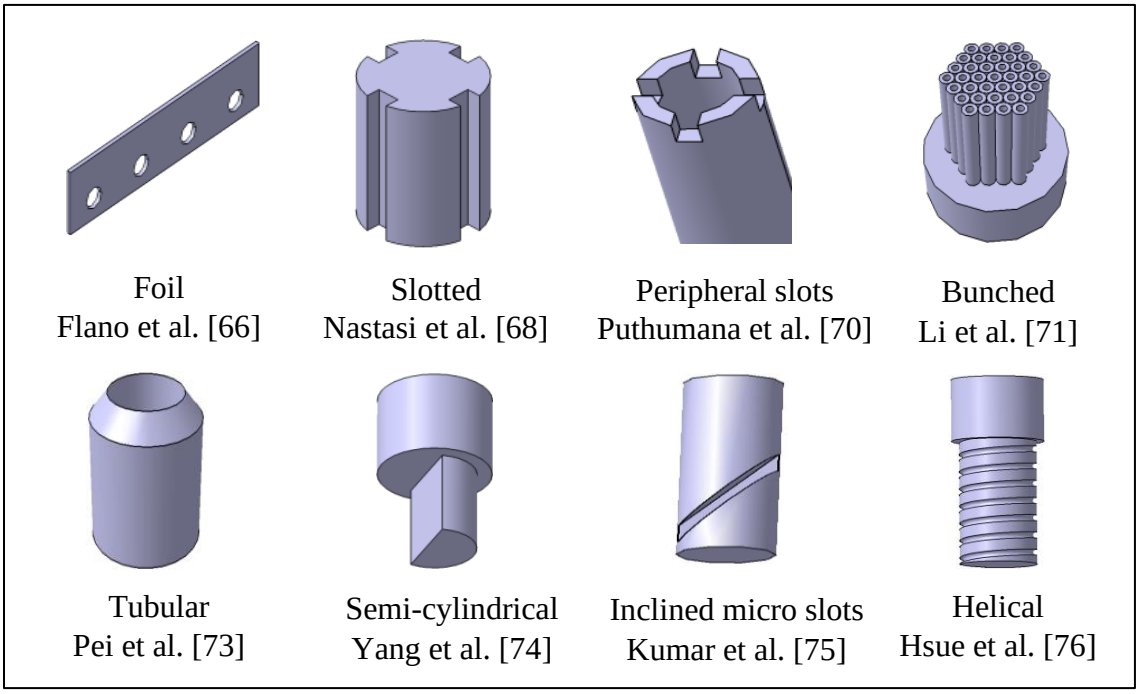

Figure 1.14 Various shapes of tools

Puthumana et al. [70] utilized peripheral slots for Dry EDM in gas to improve MRR, reduce TWR and radius overcut (ROC). The debris flushing was effective in the gap. Four peripheral slots on electrodes improved MRR, depth of cut and minimize TWR, ROC. The reduction of debris attachment on the tool electrodes was also observed. Li et al. [71] and Gu et al. [72] improved flushing efficiency in EDM using bunched electrode consisting of multi-hole inner flushing. As compared with a solid electrode consisting of mono-hole inner flushing, effective flushing is achieved using multi-hole inner flushing. This resulted in higher peak current of 127A and increases MRR by three times with relatively low TWR.

Pei et al. [73] proposed a fix length compensation ED milling using tubular tools. The truncated conic tool end is observed after machining when the tubular tool is used. The tubular tool can better control the milling depth as compared to the cylindrical tool. The

machining error is controlled within 2 % and surface fluctuation is less than 4 μm, improving the accuracy and efficiency of the process. Yang et al. [74] investigated the machining characteristics of micro holes using a semi-cylindrical tool with and without ultrasonic vibrations in micro Electrochemical machining (ECM). The semi-cylindrical tool provided more flow space for the electrolyte which resulted in 76 μm hole at a depth of 300 μm on stainless steel. With ultrasonic vibrations, machining is more effective with a reduction in machining time.

Kumar et al. [75] investigated response characteristics of micro EDD of holes by using slotted tools with inclined micro slots. They found that the need for flushing is eliminated and the slotted tool acts as a self-flushing electrode which further eliminated the occurrence of arcing and short-circuiting. The slotted electrode improved MRR, TWR, taper angle, corner radius and aspect ratio at tool speed of 1000 rpm. Hsue et al. [76] proposed a hybrid synchronized process for precision drilling and polishing using the micro-EDM grinding process (micro-EDMG). The helical micro-tool improved penetration and surface quality of the machined micro-hole. The Ra value achieved is 0.107 μm and the difference between the entrance and exit diameters of the through micro-hole is 5 μm with a depth of 300 μm.

1.5. LITERATURE GAP

1. Investigation of the flow-field in the micro domain of the ED milling is not addressed.
2. Simulation study to understand the trajectory of the debris particles of µED-milling is not addressed.
3. Investigation on the use of straight slotted tool in the µED-milling process is not observed.

1.6. SCOPE OF THE PRESENT WORK

In the µED-milling process, the simple cylindrical tool is able to cut intricate shapes due to tool rotation and motion along three directions. It is similar to the wire-EDM process, the only difference is tool rotation and it does not require a continuous supply of wire. The rotation is an inherent part of the µED-milling process and is responsible to affect the machining performance and surface characteristics. Most of the literature is focused on the MRR, TWR and statistical analysis of the µED-milling process. The machined channel is tapered at the edges and there is considerable tool wear. The physical phenomenon happening at the IEG is still unknown and needs to be further clarified. This is due to the complexity of the process where the sparking occurs in a small gap of few microns within microseconds. Hence, the present work is focused on studying the physical phenomenon happening at the IEG of the µED-milling process. Some study on this is already published in the literature. The challenge here is the size of the IEG which is of few microns. To overcome this, the CFD analysis is used to study the dielectric flow-field and debris movement in the gap. The tool rotation causes non-uniform deposition and makes the machined channel tapered at one end. The sparking behavior and dielectric flow in the IEG is captured using high-speed imaging technique. The microscopic images at high magnification is used to study the surface topography of the tool and workpiece surface. Considering the huge potential of the present technique in microfabrication, this topic has been considered for the present research. The flow chart in Figure 1.15 shows the research domain of the present work.

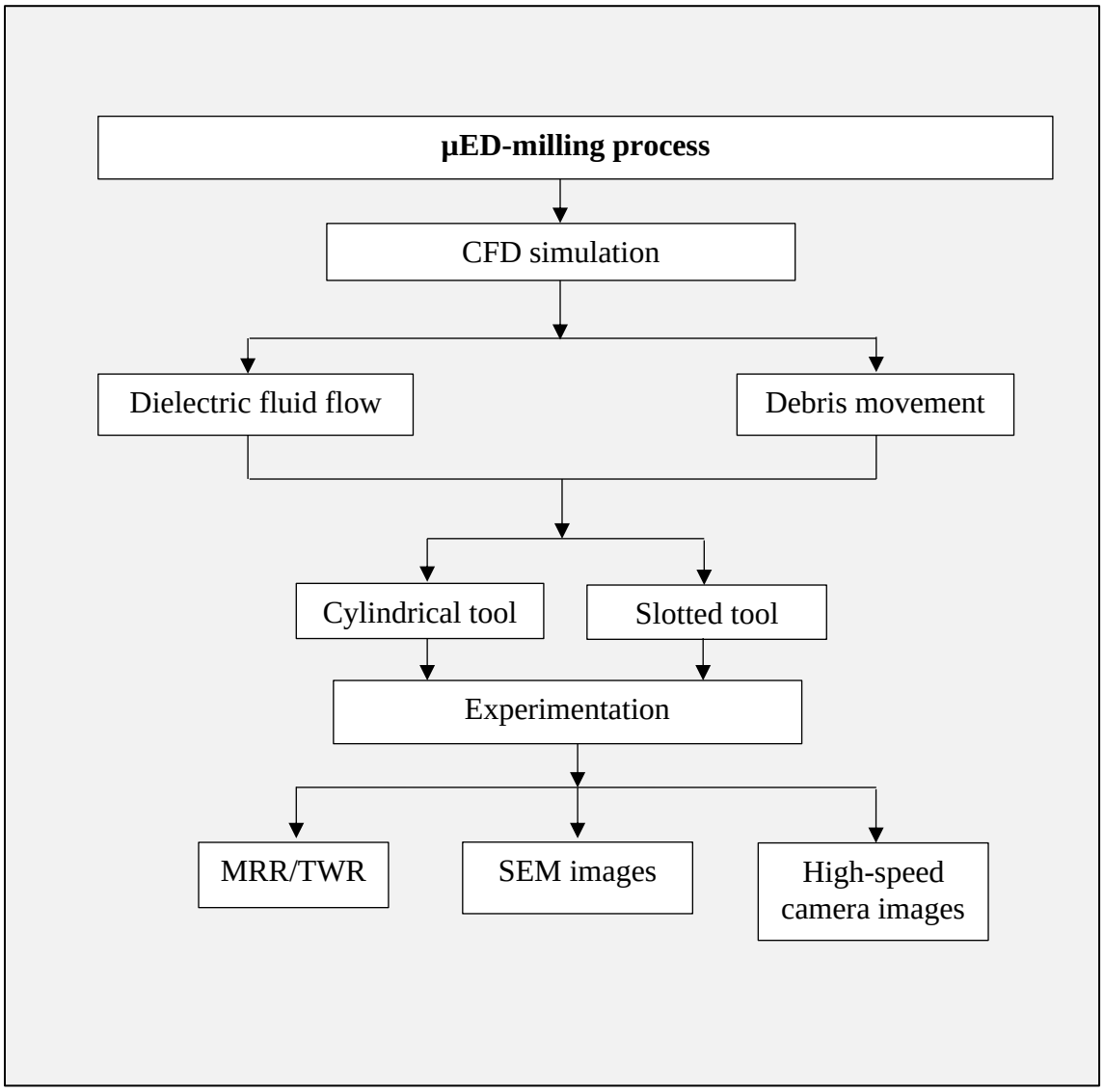

Figure 1.15 Flowchart of the research work

1.7. OBJECTIVES

The objectives of the present work are as follows,

a. To study the dielectric flow-field in the IEG of µED-milling for various input parameters such as tool rotation speed, nozzle inlet velocity, tool and workpiece geometry using simulation.
b. To study the debris particle trajectory, distance travelled and accretion rate in the IEG using discrete phase modelling.
c. To study the effect of temperature and cooling rate of the debris particles using simulation and validating with analytical method.
d. To conduct simulation using slotted tool and compare results with cylindrical tool.
e. To compare the experimental findings and surface topography of the machined µchannel for cylindrical and slotted tool.
f. To capture images of spark and dielectric flow in the IEG using high-speed technique.

1.8. ORGANIZATION OF THE THESIS

Chapter 1 is an introduction to non-conventional machining process and EDM. In EDM, the discussion pertains to the basic principle, types, and elements of EDM and the topic of research interest µED-milling. A detailed literature survey of ED-milling is presented and the survey is extended to other areas relevant to the research domain. The chapter concludes with the scope and objective of the present work and the organization of the thesis.

Chapter 2 presents the description of the CFD model used for the simulation study. The discrete meshing of different zones and the boundary conditions are discussed in detail. The details of different algorithms used for the simulation is discussed.

Chapter 3 is a CFD analysis of the dielectric flow-field in the IEG. The characteristics of different dielectric and the analysis points of the simulation model are

discussed. The effect of different input variables on the dielectric fluid flow and the velocity in the IEG is discussed with the contour plots.

Chapter 4 discusses the movement of debris particle in the IEG. The discrete phase modeling is used to study the trajectory of the particles. The accretion of the particles injected from different positions of the gap is presented with a contour plot. In the end, the analytical and simulation study of cooling rate of debris particle is discussed.

Chapter 5 extends the study of CFD simulation to slotted tool. The discussion pertains to the dielectric flow and debris movement in the IEG using similar input variables used for cylindrical tool.

Chapter 6 presents the experimental work to compare the machining performance such as MRR and TWR using cylindrical and slotted tool. The specification details of the hybrid μEDM machine and the setup used for the experimental work is presented. The high-speed camera images of the spark, dielectric flow and the SEM micrographs of the debris and machined μchannel is presented.

Chapter 7 presents the main conclusion of the work and scope for future study.